Advection-Dominated Transport Dynamics of Pili and Flagella-Mediated Motile Bacteria in Porous Media

Marc Berghouse[†,‡], Lazaro J. Perez[‖], Andrew Plymale[+], Timothy D. Scheibe[++] , & Rishi Parashar[†,*]

† *Division of Hydrologic Science, Desert Research Institute, Reno, Nevada, 89512*

‡ *Graduate Program of Hydrologic Sciences, University of Nevada, Reno, Reno, Nevada, 89557*

‖ *Department of Civil and Construction Engineering, Oregon State University, Corvallis, Oregon, 97331*

+ *Energy and Environment Directorate, Pacific Northwest National Laboratory, Richland, Washington, 99354*

++ *Earth and Biological Sciences Directorate, Pacific Northwest National Laboratory, Richland, Washington, 99354*

Corresponding Author: Rishi Parashar

Email: Marc.Berghouse@dri.edu, lazaro.perez@oregonstate.edu, plymale@pnnl.gov, tim.scheibe@pnnl.gov, Rishi.Parashar@dri.edu[*]

Phone Number of Corresponding Author: +1 775 673 7496

Author Contributions: R.P. and T.D.S. designed research. L.J.P performed experiments. A.P. cultured bacteria and advised on biological aspects of the experiments. M.B. conducted simulations of microfluidic models and analyzed experimental data. M.B., L.J.P., and R. P. interpreted the modeling results. M.B., L.J.P., R.P., and A.P. wrote the paper.

Competing Interest Statement: The authors declare no competing interests.

Preprint Server: N/A

Keywords: Bacterial Transport, Motility, Porous Media

Abstract

The transport of motile bacteria in porous media is highly relevant to many fields, ranging from ecology to human health. Still, critical gaps remain in our understanding of the impacts of hydrodynamics and pore structure on bacterial transport. Here, we present direct visualizations of three species of motile bacteria under variable flow rates and porosities. We find that at higher flow rates, motility is less critical to the transport of bacteria, as motion is controlled by hydrodynamic advection, making it difficult for bacteria to move across streamlines. We show that this lack of motion across streamlines results in increased velocity autocorrelation and bacterial spreading in the direction of flow. Furthermore, we find that transport of bacteria with different motility types are impacted by flow rates to different extents. At low flow rates, the transport of bacteria with pili-mediated twitching motility is strongly controlled by advection, whereas bacteria with flagella still display active motility. At higher flow rates, we show that bacteria with peritrichous flagella maintain their motility characteristics to a greater degree than bacteria with pili or monotrichous flagella. We also examine experimental net speeds of bacteria in relation to the simulated flow fields and find that the interactions between hydrodynamics, motility, and porous media geometry lead to oversampling of medium-velocity regions of a pore network by all three species. The study presents new perspectives on how different types of motile bacteria are transported and dispersed in porous media aided by strength of differentially advecting fluid.

1. Introduction

Motile bacteria often live in dynamic flow environments, and their migration involves complex self-propulsion strategies that are relevant to human health and ecology [1–3]. Navigating confined spaces of a pore network, motile bacteria employ diverse movement modalities (e.g., turn angles, run-and-tumble, or run-and-flick) that characterize their migration [4–9]. In porous media, the degree of confinement (i.e., porosity) and speed of the fluid flow strongly affect bacterial migration and modulate their interactions with the surrounding environment. This, in turn, has a broad range of effects on bacteria, such as altering their movement [10], behavior [11], resource acquisition [12], and signaling [13], thereby influencing their metabolic functions, spatial distribution, and diversity. Spatial variations in flow velocities and the related changes in shear add another level of complexity to the transport of bacteria. Transverse movement of bacteria from low-shear to high-shear regions located near surfaces has been shown to result in the accumulation of cells in low-velocity regions [14, 15]. This phenomenon, termed shear trapping, has been identified as one major mechanism that drives initial colonization of curved surfaces and microfluidic pore channels [16–18], leading to the formation of suspended biofilm structures [19, 20]. While these observations have led to improvements in our understanding of bacterial transport in idealized systems, there are significant gaps in our ability to quantify and predict transport behavior under complex conditions, such as in pore networks designed to produce the hydrodynamics of natural porous media. Understanding the motile behavior of bacteria in confined environments, in which they search for available physical space and move in response to fluid flow, has implications for a wide range of applications, such as bioremediation [21], biofilm formation [22, 23], and anticancer drug delivery [24].

Here, we report direct bacterial transport visualizations, at single-cell resolution, of three different species of motile bacteria under variable flow conditions in a quasi-2D porous media with different levels of pore

confinement. Recent research conducted in microfluidic porous chips has shown that while transport of non-motile bacteria is compact giving rise to a Gaussian distribution of traveled distances (i.e., follows streamlines with negligible retardation due to mass exchanges between fast and slow moving zones), the distribution of motile strains in the pore spaces show both active retention and enhanced dispersion due to exchanges between fast flow channels and low velocity regions closer to the grain surfaces [17, 25]. The presented work here examines the transport dynamics of three motile species with an overarching goal of highlighting key statistical differences in various transport metrics so that more informed modeling approaches can be developed for upscaled transport simulations. Having an improved understanding of dispersion rates and of the key factors that control dispersion, such as the velocity and turn angle distributions, would provide robust ingredients for development of random walk based approaches [25]. We focus on investigating three rod-shaped bacteria – *Acidovorax* strain JHL-9 [26], *Geobacter sulfurreducens* [27], and *Paenibacillus* strain 300A [28] – due to their common attribute of metal-reducing capabilities. By studying these specific microorganisms, our research findings are especially relevant to bioremediation and biogeochemical cycling in terrestrial environments [29-31]. The three bacteria show slight variations in size – *Acidovorax* has an average body size of 10.1 ± 2.2 μm, *Geobacter* is about 8.2 ± 1.0 μm, and *Paenibacillus* is the largest at 14.5 ± 7.3 μm. Furthermore, our selection of these species is based on their distinct modes of motility. Using their pili to attach to surfaces and pull themselves towards new locations [32], *Geobacter sulfurreducens* exhibit twitching motility [33]. *Paenibacillus* 300A exhibit swimming motility, presumably driven by peritrichous flagella [34]. *Acidovorax* JLH-9 [26] exhibit twitching motility, consistent with genomic analysis of the strain, though transmission electron microscopy (TEM) images of the strain suggest the presence of polar/monotrichous flagella, indicating the possibility of swimming motility as well. Swimmers generally move much faster than twitchers [32, 35-37], providing a reasonable basis in this study to compare the two different motility types at different flow rates. The primary focus of this paper is not to decipher the fundamental reasons for differences in the transport behaviors of the three selected species, but rather to evaluate transport characteristics of bioremediation relevant species with different motility types in order to help lay a framework for species-aware upscaling and macroscale transport simulations.

We find that regardless of the motility type, as flow rates increase, individual cells have trouble in moving across streamlines, resulting in weaker coupling between bacterial motility and their overall transport characteristics. We show that as flow speed increases, bacteria disperse faster in the direction of flow, due to a lower likelihood of motion across streamlines and an increase in longitudinal displacement driven by differentially advecting fluid in a porous environment. In other words, the distance between individual cells grows at a fast rate since cells are less likely to make transverse movements (i.e., displacements across streamlines), and are more likely to move longitudinally at a range of velocities produced by the parabolic nature of laminar flow profiles. Furthermore, we show that the motility of *Paenibacillus* is less impacted by flows in porous media than the motilities of *Geobacter* and *Acidovorax*, highlighting the strength of peritrichous flagella-driven motility. Additionally, we provide evidence that motile bacteria tend to oversample medium-velocity zones in porous media for the flow conditions tested in our experiments. This work thus provides an improved picture of the transport of motile bacteria in confined porous media under variable flow rates, especially in relation to the impact of flow on different motility types, with implications for several applications where an understanding of pore-scale transport and upscaling of bacterial transport is desired.

2. Materials and Methods

2.1 Bacterial Transport in Microfluidic Devices

To investigate the impacts of porosity, flow rate, and motility on bacterial transport, we recorded high-resolution videos of three species of bacteria swimming in microfluidic devices [2,000 μm width × 20 μm height ($w \times h$)] at flow rates of 0 μL/h (no flow), 1 μL/h and 5 μL/h. The chosen flow rates allow for comparative analyses of bacterial transport for the control condition of no-flow, and when the magnitude of flow speeds and bacterial motility speeds are of a similar order. The micromodels were made from polydimethylsiloxane (PDMS) and contained staggered pillar arrays of different grain diameters and pore lengths, resulting in either low porosity ($\phi = 0.42$) or high porosity ($\phi = 0.60$) micromodels. The mean fluid speeds (v_m) determined from flow rate (Q), cross-sectional area (A), and porosity (ϕ) as $v_m = Q/A\phi$, in the low porosity geometries were 16.5 μm/s and 82.7 μm/s, and the mean fluid speeds in the high porosity geometries were 11.6 μm/s and 57.9 μm/s, for the low and high flow rates, respectively. These correspond to fluid speeds in the range of 1 m/day to 7.15 m/day which are medium to high speed values typically observed in bioremediation applications in alluvial aquifer settings [38, 39]. Assuming a length correlation scale based on the size of the pore lengths in our porous geometries, we find that Reynolds numbers in our experiments are in the range of 10^{-5} to 10^{-3}. We found conducting experiments at lower flow rates (< 1 μL/h) in our micromodels challenging due to pump limitations in establishing extremely low uniform rates and difficulties encountered by emergence of small drift speeds even in absence of external flow gradients presumably due to imperfections in model fabrication, small pressure aberrations at the inlet/outlet ports, small axial tilts, or potential presence of extracellular polymeric substance gradient [40]. Using pore throat length (given in section 2.2) as the characteristic length, and using the values of dispersion coefficients presented later in section 3.1.2, the velocities generated in the experiments would result in Peclet numbers approximately in the range of 0.25 to 16 – a range that allow us to make broad observations though they may be not fully generalizable. Experiments at no-flow condition in an open environment (i.e., without granular obstacles) were conducted with a subgroup of species in a previous work [41], which provides insights into the species-aware departure from Fickian diffusion in unconfined environments. After recording the videos from several replicates of experiments, we used TrackMate [42] to track, extract, and reconstruct thousands of trajectories (ranging in length from low tens of microns to several hundred microns) of individual cells (Fig. 1).

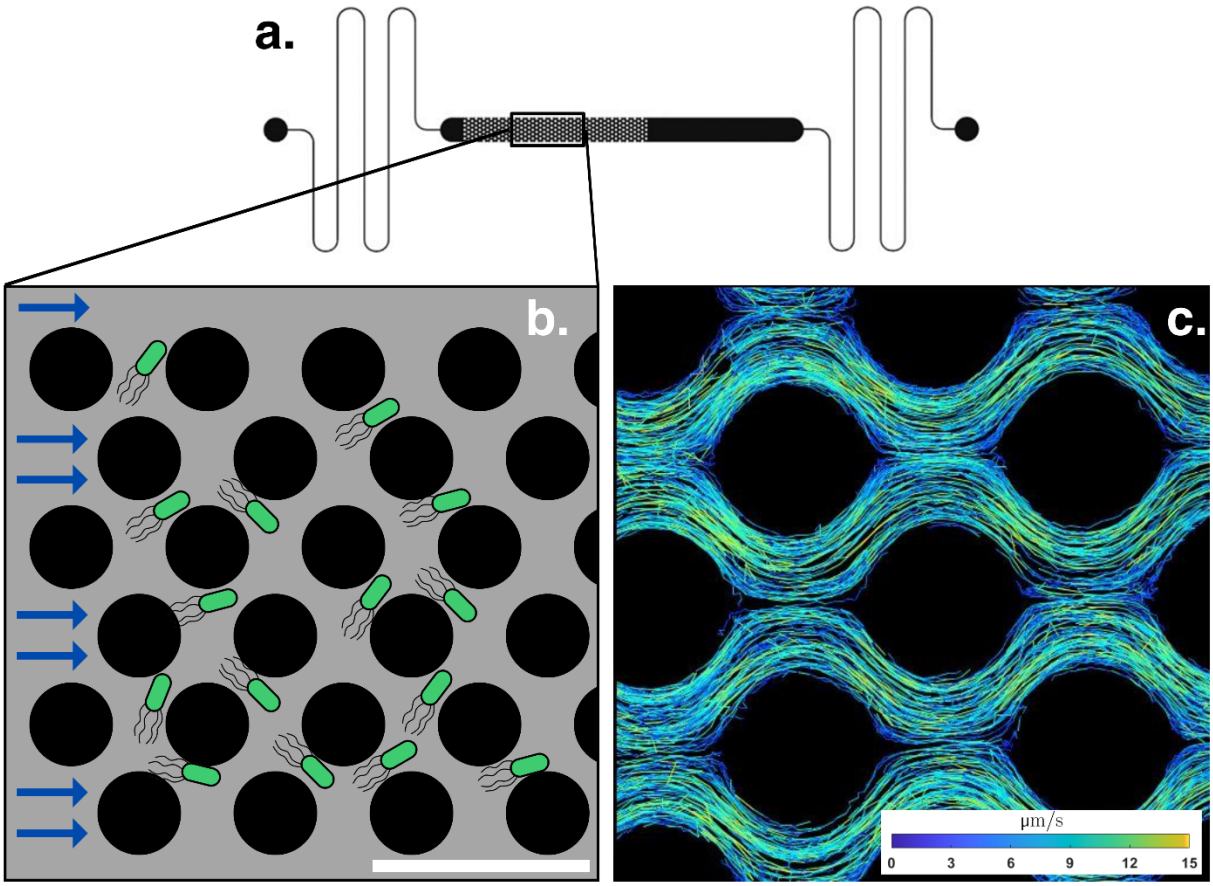

Figure 1. Experimental setup used to analyze bacterial transport in microfluidic devices. **(a)** A sketch of the full micromodel from [41], which used the same basic micromodel schematic as our experiments. The left black dot represents the inlet and the right dot represents the outlet. The black section represents an unobstructed part of the micromodel, and the gray section represents the part of the micromodel with cylinders. **(b)** Depiction of bacteria flowing (from left to right) through a section of the high porosity ($\phi = 0.60$) micromodel. The gray space represents the channels that fluid and bacteria travel through, and the black circles represent the cylinders (also referred to as "grains"). The scale bar represents 120 μm. Bacteria are not drawn to scale. **(c)** Bacterial trajectories for *Acidovorax* obtained in 5-minute interval over the course of the experiment in the high porosity micromodel at a flow rate of 1 μL/h. The colormap represents net speed of bacteria, with warm colors representing high speeds and cool colors representing low speeds.

To account for the small drift observed in no-flow experiments from one end of the micromodel to the other, we calculated the background flow (drift speed) by computing the rate of change in the location of the centroid as $v_d = \frac{1}{k}\sum_0^k \frac{d}{dt}(r_{cm})$, where r_{cm} is the center of mass (x and y positions) of all bacteria in a frame at no-flow, and k is the number of frames (in our case, $k = 30$). To include the greatest number of possible trajectories for this calculation, we reset the starting point of all trajectories to $t = 0$. We calculated mean drift speeds for *Acidovorax* (0.29 μm/s), *Geobacter* (1.41 μm/s) and *Paenibacillus* (0.59 μm/s)

separately. These drift speeds are significantly small compared to the speeds produced in the low-flow and high-flow experiments thus allowing us to treat the transport of bacteria in the two flow experiments as being solely driven by the interplay between motility and hydrodynamics.

Transport characteristics of bacteria were quantified using net speeds $|v_n| = \frac{\sqrt{(x_{t+1}-x_t)^2+(y_{t+1}-y_t)^2}}{\Delta t}$, turn angles $\alpha_t = tan^{-1}\left(\frac{y_{t+2}-y_{t+1}}{x_{t+2}-x_{t+1}}\right) - tan^{-1}\left(\frac{y_{t+1}-y_t}{x_{t+1}-x_t}\right)$, mean square displacement $MSD(t) = \frac{1}{N}\sum_{i=1}^{N}|r_i(t) - r_i(0)|^2$, velocity autocorrelations $C_v(\tau) = \langle|v_n|(t+\tau)\cdot v(t)\rangle$, average effective dispersion coefficients $\overline{\overline{D^e}}(t) = \frac{1}{w\phi}\int_0^w D^e(t,y')dy'$, and bivariate angle-speed probability density contours. Here x_t and y_t are individual bacteria positions at time t, N is the total number of tracked cells, r_i is the displacement for bacterium i, and $|v_n|$ is the magnitude of the net velocity (i.e., speed) of the bacteria. D^e reflects the dispersion coefficient for each discrete bin in the y-direction of the domain used to calculate the average effective dispersion coefficient and is defined as the second moment of the center of mass of the particles. The scripts used to calculate all statistics can be found in Supplementary Methods 2. Note that the net speeds are the speed of the bacteria determined through particle tracking. Since bacteria are displaced through the porous media both due to their own motility and the advection imparted by the background flow, the net speed obtained via particle tracking measures the combined effect of these two drivers.

2.2 Micromodel Construction

Micromodels for three porous geometries were constructed from PDMS using staggered arrays of grains to represent porous media (see Fig. 1). The three geometries used in this experiment were **(1)** arrays with a grain diameter (GD) of 80 μm and a pore throat length (PL) - minimum space between grains - of 20 μm ($\phi = 0.42$), **(2)** arrays with a GD of 40 μm and a PL of 20 μm ($\phi = 0.6$), and **(3)** arrays with a GD of 40 μm and a PL of 10 μm ($\phi = 0.42$). The micromodel dimensions were 2 mm in the transverse direction, 17 mm in the longitudinal direction (for the porous section), and 20 μm in the vertical direction. We chose a depth of 20 μm as we found that a larger depth causes bacteria to move in and out of the focal plane of our camera too often, and constraining the depth further would have caused excessive shear along the vertical plane.

2.3 Bacteria Culture

Bacterial strains *Acidovorax* JHL-9 and *Paenibacillus* 300A were grown in liquid culture aerobically at 30 °C on dextrose-free Trypticase Soy Broth (TSB). At late-log to stationary phase, cultures were diluted to an optical density at 600 nm (OD600) of ~ 0.1 – 0.15 and injected into the micromodel devices described above. *Geobacter sulfurreducens* was grown anaerobically (80:20 N_2:CO_2), in glass serum bottles or headspace vials, crimp-sealed with butyl-rubbers stoppers, on Freshwater Medium [43] with 50 mM sodium fumarate as electron acceptor in place of ferric citrate [44]. Stationary-phase *G. sulfurreducens* cells were injected, without dilution, into micromodel devices that had been de-oxygenated overnight in an H_2-free anoxic chamber (MBraun, O_2 < 10 ppm, 100% N_2). De-oxygenated micromodels were then removed from the anoxic chamber using an anaerobic jar and were kept in the anaerobic jar until immediately before use. *G. sulfurreducens* cells were removed from the serum bottle or headspace vial with a degassed (80:20 N_2:CO_2) 1-cc syringe and 22-gauge needle and immediately injected into the degassed micromodel. Though our video acquisition was generally restricted to about an hour after the injection of bacteria, it

should be noted that *G. sulfurreducens* are also known to tolerate and grow with oxygen as a terminal electron acceptor for up to 24 hours [45].

2.4 Video Acquisition

All videos were collected with a confocal imaging technique on a Nikon Eclipse Ti2-U inverted microscope equipped (viewing vertically downwards and recording motion in the x-y plane) with a digital CMOS camera Hamamatsu Orca-Flash 4.0 controlled by NIS Elements imaging software. The sensor pixel size was 6.5 μm x 6.5 μm, and each recorded frame had a size of 2048 pixels x 2048 pixels. For videos at 10x magnification, the recorded domain size was 2048 x 6.5/10 = 1331.2 μm x 1331.2 μm, and for videos at 20x magnification the video domain was 665.6 μm x 665.6 μm. Videos were recorded for 5 minutes at frame rates of about 10 frames per second (the interval time between frames varied slightly resulting in rates of 8-12 frames per second). The exact time interval between frames were recorded to allow for accurate computation of transport metrics.

2.5 Image Preprocessing

The raw videos were preprocessed with background subtraction using a lag method specifically developed in-house for these experiments. To capture trajectories of bacteria that may have not moved between two successive frames, the subtracted background must be more than a few frames back in time. Standard practice in background subtraction for such cases is to use the initial frame, or the mean frame, as a background for the rest of the video, but this was not possible in our case due to variability in image brightness throughout the duration of the video. To get around these problems, we used the 5th previous frame to perform background subtraction. In other words, to subtract the background of frame 6, we calculated frame 6 minus frame 1. Thus, any bacteria that moved a little over the course of 5 frames could still be identified in particle tracking.

2.6 Particle Tracking

After background subtraction, the foreground was then loaded into ImageJ and particle tracking was performed with the plugin TrackMate. For feature detection the Laplacian of Gaussian (LoG) detector was used, and to link the features, we used the Linear Assignment Problem (LAP) tracker. A sample output of trajectories from TrackMate is given in the Supplementary Data.

2.7 Flow Field Simulations

Simulations of the flow field were conducted to understand which parts of the geometry bacteria are likely to oversample or undersample. The experimental geometry was initially digitized in Blender then refined in OpenFOAM to produce a regular grid consisting of 2400 x 2400 x 72 voxels with a resolution of $\Delta x = \Delta y = 0.2773$ μm, $\Delta z = 0.2778$ μm. The flow fields of the digitized geometries were obtained by solving the flow of incompressible Newtonian fluid governed by the Navier-Stokes equations using SimpleFoam. The steady-state solver belongs to the OpenFOAM package that uses semi-implicit methods for pressure linked equations algorithms. Constant flow rate at specific experimental values of 1 and 5 μL/h ($Q = 2.78 \times 10^{-13}\mathrm{m}^3\mathrm{s}^{-1}$ or $Q = 1.39 \times 10^{-12}\mathrm{m}^3\mathrm{s}^{-1}$) and constant pressure $P = 0\ \mathrm{kg\ m}^{-1}\mathrm{s}^{-2}$ were imposed at the inlet and outlet of the domain, respectively. No-slip conditions were assigned to the fluid-solid interface. We used a kinematic viscosity ν of 1.14x10^{-6} m^2/s for the fluid (TSB), given a calculated ratio of

ν_{TSB}/ν_{water} of 1.14 [46]. A sample case folder for the simulations, as well as the commands used to run it on a local machine, can be found in Supplementary Methods 1.

3. Results

3.1 Advection-Dominated Transport Dynamics

We use the term "advection-dominated transport" to highlight a regime wherein the variable shear forces within pore spaces, and dominance of flow speeds over motility speeds, restrict the ability of bacteria to move across streamlines, thus guiding their motion primarily along streamlines at differential velocities. Advection-dominated transport would occur in scenarios of high Peclet number [47] and persists in situations where weak coupling between motility and biofilm formation patterns are observed [48]. This type of transport, guided by shear induced cell rotation causing decreased transverse dispersion and increased lateral dispersion, has also been previously reported for bacteria in porous media flows [49]. Here, we provide additional relevant statistical information to characterize advection-dominated transport for three different species of motile bacteria relevant to bioremediation applications. In the following, we characterize transport dynamics through the (MSD), turn angle distribution, $C_v(\tau)$, and $D^e(t)$. We use these statistics to develop a robust understanding of transport driven by differential advection, movement across streamlines, velocity decorrelation, and spreading [50, 51].

3.1.1 Turn Angle Analysis Reveals Impact of Flow Rate on Motility

To understand the motility of each species of bacteria, we primarily use their turn angle distributions. Note that turn angles as defined in this paper are not the same as traditionally reported turn angles that reflect the body orientation during bacterial run and tumbles [52]. Because the bacterial speeds are not significantly greater than the background flow speeds, and because our experiments were performed at a relatively low frame rate, we use the term "turn angle" to capture the relative change in the trajectory of advected cells between successive video frames.

For no-flow conditions, *Paenibacillus* (peritrichous flagella-based motility) show a high probability of low or very high turn angles (Fig 2a). Low turn angles ($\alpha > -30°$ *or* $\alpha < 30°$) would represent persistent forward motion (i.e., long run times), and high angle turns would represent reversals in direction (i.e., tumbling). Although not a necessary condition, a high probability of low turn angles implies a high probability of runs, and a high probability of medium to high turn angles implies a high probability of tumbling. *Geobacter* and *Acidovorax* (pili or monotrichous flagella-based motility) have a relatively low probability of both low and high turn angles because their motion is generally more random and is subject to slight changes in hydrodynamics.

To identify the differences in motility for each species more effectively, we also report the ratio of the turn angle PDF for each species to the turn angle PDF for *Geobacter* (Figs. 2d-2f). Essentially, *Geobacter* represents our twitching baseline, as their speed distributions (Supplementary Figure 1) and mean speed (about 2.3 μm/s after subtracting average drift) are generally in agreement with previously reported twitching speeds of various bacteria [32, 35-37]. Thus, the PDFs of *Acidovorax* and *Paenibacillus* turn angles show departure of their motion behavior from a typical twitcher. When flow is absent (Fig. 2d), the PDF ratio for *Paenibacillus* shows exactly what we expect from a swimmer – high probability of low turn angles (persistent forward motion), low probability of medium turn angles (random motion), and high

probability of high turn angles (direction reversal). Intriguingly, the genome of *Acidovorax* JHL-9 (see data availability) contains numerous genes related to twitching motility but not a complement of genes related to flagella-mediated motility. However, as previously discussed, wet mount TEM images of strain JHL-9 (Supplementary Figure 2) suggest the presence of polar flagella. Furthermore, the speed (Supplementary Figure 1) and turn angle ratio (Fig. 2d) distributions at no-flow indicate that *Acidovorax* behaves differently than *Geobacter* and closer to *Paenibacillus,* thus revealing distinct motility traits to the three species selected in this study.

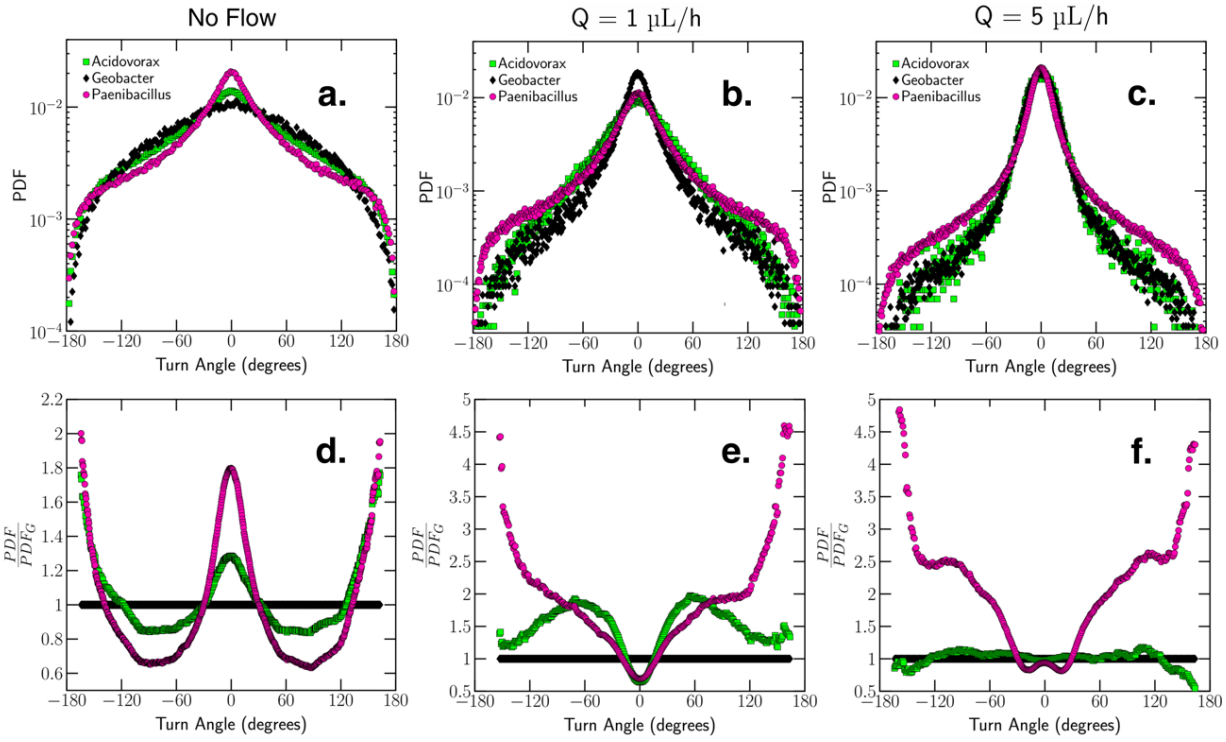

Figure 2. Turn angle PDFs for all three species in the low porosity geometry (grain diameter = 80 μm, pore length = 20 μm). **(a)** Turn angle PDF at flow rate of 0 μL/h. **(b)** Turn angle PDF at flow rate of 1 μL/h. (c) Turn angle PDF at a flow rate of 5 μL/h . (d) Turn angle PDF ratio at a flow rate of 0 μL/h. € Turn angle PDF ratio at a flow rate of 1 μL/h. (f) Turn angle PDF ratio at a flow rate of 5 μL/h. Turn angle PDF ratios are calculated as the PDF/PDFG, where PDFG represents the PDF of Geobacter. We choose to make the ratios relative to *Geobacter* as they move much less than the other bacteria. Convergence of the shape of the turn angle distribution and clustering of turn angles around 0° at 5 μL/h indicates strong advection-dominated transport.

Compared to the case of our no-flow experiments, the interpretation of our turn angle distributions in the presence of flow is slightly more complicated. We posit that in a viscous steady-state flow, non-motile bacteria would behave as inert particles transported by advection only, thus moving along streamlines of the pore-scale flow field, which would result in small turn angles between successive steps of the trajectories. In other words, in presence of a background flow, persistent forward motion means a high probability of low turn angle distributions. However, motile bacteria also move across streamlines, move

in reverse direction, and explore the pore space under flow conditions, and as a result, large turn angles should be expected for highly active self-propelled bacteria [25, 53-5].

We find that *Paenibacillus* have a higher probability of large turns ($\alpha < -90°$ *or* $\alpha > 90°$) than the other two species at a flow rate of 1 μL/h, while at 5 μL/h this difference is even more noticeable (Figs. 2b and 2c). Examining the turn angle PDF ratios (Fig. 2e), we see that at 1μl/h *Paenibacillus* and *Acidovorax* have similar distributions for low to medium turn angles, but *Paenibacillus* has a much higher probability of large turn angles, indicating a greater potential for direction reversal than the other bacteria. At 5 μL/h (Fig. 2f) the similarities between *Paenibacillus* and *Acidovorax* completely disappear, and the turn angle PDFs for *Acidovorax* and *Geobacter* essentially converge. This implies that at high flow speeds, *Paenibacillus*, with its peritrichous flagella, are either able to tumble more, or run faster, than *Acidovorax* or *Geobacter*. Furthermore, these results suggest that *Acidovorax,* with its monotrichous flagella, experience a greater impact on its motility due to flow speed than *Paenibacillus* do. While more experiments with a greater variety of monotrichous and peritrichous species are needed to confirm this trend, our initial results imply that peritrichous flagella enable motility at higher flow speeds than monotrichous flagella. Since the no-flow speed PDFs show that *Acidovorax* and *Paenibacillus* have similar max speeds, and monotrichous and amphitrichous bacteria have generally been shown to be capable of higher speeds than peritrichous bacteria [36, 58], it does not seem likely that the difference in motility between *Acidovorax* and *Paenibacillus* at high speed is due to run speeds. Thus, our results also imply that at high flow rates *Acidovorax* are unable to tumble, but *Paenibacillus* can. This is supported by research showing that increasing numbers of flagella increases the probability of tumbling [59]. However, we should also note that differences in the flagellar architecture are not the only possible explanations for differences in the turn angle distributions. Two other possible explanations for this include reorientation strategies, which may impact their preference to run or tumble [60], and size-related dynamics, which have been shown to influence hydrodynamic impacts on bacterial motility [61]. As discussed in the introduction, the *Geobacter* and *Acidovorax* have similar body lengths, indicating that size is an unlikely explanation for the differences observed between these two species. However, the body sizes of *Paenibacillus* are much larger than those of *Geobacter* and *Acidovorax*, indicating that the differences in overall transport observed for *Paenibacillus* may in part be due to their larger body size. Regardless of the exact cause, our results do show that *Paenibacillus* can maintain swimming-like behavior at higher flow rates. *Acidovorax*, on the other hand, act like swimmers at low or no flow, and twitchers at high flow. In other words, advection-dominated transport, which causes trajectories of swimmers to appear similar as trajectories of twitchers, occurs at a lower flow rate for *Acidovorax* than for *Paenibacillus*.

3.1.2 Effect on Bacterial Spreading at Different Porosities and Flow Rates

Figure 3 confirms additional evidence of advection-dominated transport via the computed MSD. Here, we introduce the term “differential advection” to describe the MSD results, stemming from the bacteria's mixed super-diffusive motions influenced by streamline shifts, trapping, and pore space exploration. This term aptly captures the relationship between velocity decorrelation events and bacterial advection and offers a nuanced understanding of the transport dynamics. As the flow rate increases, bacteria will, on average, have a larger range of displacements due to the magnitudes of velocities it can sample within the laminar profile of porous media flow [17]. Furthermore, smaller turn angles at higher flow rates (as described in the previous section) implies less streamline changing. This results in higher values of the MSD driven by

increased differential advection as bacteria are transported by a range of velocities produced by converging and diverging streamlines within the pore network. Another way to think about "differential advection" is that parabolic flow velocities in porous media result in some streamlines that are on average faster than others. The diverging and converging pattern specific to the streamlines of our porous geometry even further increase the variability in speeds, which can be observed in the MSD as a large increase in the advection for bacteria that enter a state of shear mediated transport between 1 µL/h and 5 µL/h. In other words, "differential advection" results in a greater-than-expected increase in the MSD due to the impacts of shear-mediated transport which reduce streamline changing meaning the fastest particles in the fastest streamlines will advect much more quickly than if they retained their ability to change streamlines. These observations are further used for later comparisons in the context of Fig. 6, and generally align with enhanced dispersion reported due to transport of bacteria along faster flow paths than the local flow [17, 25].

Complementing the increased differential advection, as the flow rate increases, the MSDs of all species of bacteria in the low porosity geometry show signs of convergence (both in slope and magnitude as seen in Fig. 3e), likely driven by decorrelation of cell swimming as bacteria navigates pore structures [56]. Essentially, advection-dominated transport is thus revealed by the convergence (between different species of bacteria) of both turn angle distributions and MSD, and a shift toward greater differential advection. In contrast, with the high porosity geometry, we observe less evidence of MSD convergence, which indicates that the flow speeds are not high enough to suppress bacterial motility, leading to a reduction in differential advection as shown by lower MSD values (Figs. 3b and 3c). We also find that for a fixed porosity and flow rate, *Geobacter* and *Acidovorax* always advect more than *Paenibacillus*, further supporting the idea that peritrichous swimmers are differentially advected to a lesser degree than twitchers or polar swimmers.

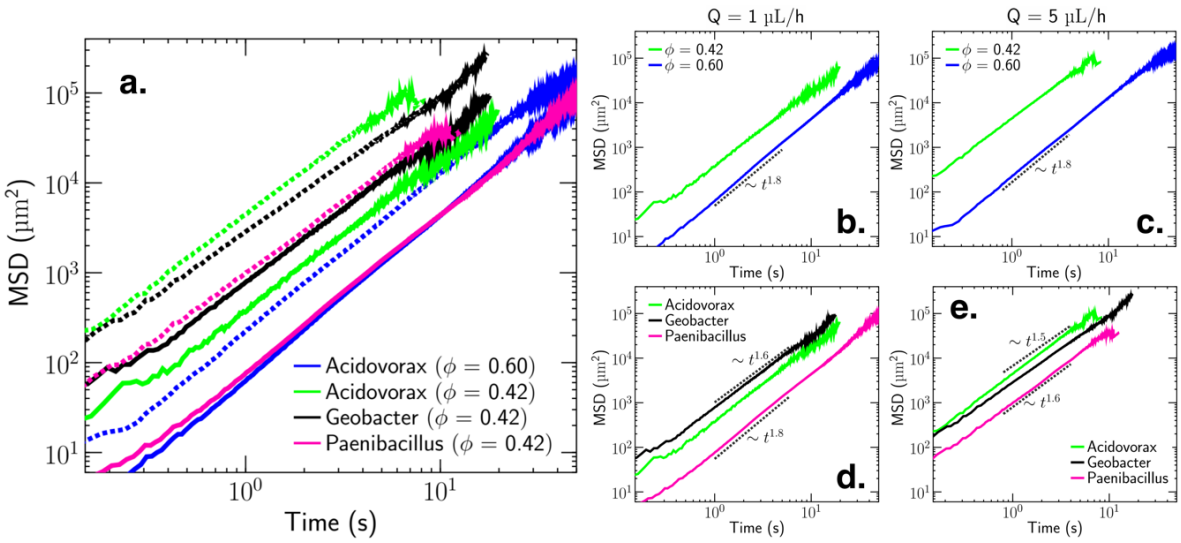

Figure 3. Mean square displacements (MSDs) at different porosities and flow rates for three different species of bacteria. **(a)** MSDs from relevant experiments (3 species at lower porosities and 1 at higher porosity, 2 flow rates).

The 1 μL/h results are shown as solid lines and the 5 μL/h results are shown as dotted lines. **(b)** MSDs for *Acidovorax* for $\phi = 0.60$ and $\phi = 0.42$ at a flow rate of 1 μL/h (mean fluid speed of 11.6 μm/s and 16.5 μm/s respectively). **(c)** MSDs for *Acidovorax* for $\phi = 0.60$ and $\phi = 0.42$ at a flow rate of 5 μL/h (mean fluid speeds of 57.9 μm/s and 82.7 μm/s respectively). **(d)** MSDs for all species for $\phi = 0.42$ at a flow rate of 1 μL/h **(e)** MSDs for all species for $\phi = 0.42$ at a flow rate of 5 μL/h. These figures show an increase in the impact of differential advection for motile bacteria as the flow rate increases. The rapid increase in MSD driven by differential advection, along with convergence of the MSDs in the low porosity geometry at 5 μL/h, provide evidence of advection-dominated transport. At both flow speeds, *Paenibacillus* show lower values of MSD than *Geobacter* or *Acidovorax*, indicating a stronger resistance to advection-dominated transport. All low porosity results in this figure are from the grain diameter = 80 μm, pore length = 20 μm geometry.

To further understand spreading in our experiments, we calculated the effective dispersion coefficient, D^e, based on the average spatial variance of the bacteria distribution evolving from a point-like injection, that is, the transport of Green function as defined in [62, 63]. At 1 μL/h, D^e is impacted by spreading in both the longitudinal and transverse directions for *Paenibacillus* and *Acidovorax*, but primarily in the longitudinal direction for *Geobacter* owing to its considerably lower twitching speed than the mean fluid speed. At 5 μL/h, D^e primarily represents longitudinal dispersion for all species. Our results show that when the flow rate increases from 1 μL/h to 5 μL/h, D^e increases the most for *Geobacter*, and the least for *Paenibacillus* (Table 1). Because *Paenibacillus* are able to maintain some form of motility at 5 μL/h, and as a result are still able to change streamlines and explore the pore space, differential advection has less of an impact on their dispersion than it does for the dispersion of *Geobacter* and *Acidovorax*. In other words, the bacteria that follow streamlines or explore less space in the transverse direction to the flow, advect and spread more in the direction of flow. These results complement those presented in [17, 25, 49], which showed that hydrodynamic gradients in porous geometries reduce transverse dispersion. We further this research by showing that bacterial transport is advective-dominated for a wide variety of flow rates depending on the type of bacterial motility.

Table 1. Effective Bacterial Dispersion Coefficients D^e ($\mu m^2/s$) for all experiments conducted in the low porosity geometry ($\phi = 0.42$). As flow rate increases, *Geobacter* have the greatest increase in dispersion and *Paenibacillus* have the smallest increase in dispersion. As the motility speeds of the bacteria are less than the fluid speed at 5 μL/h, dispersion is almost entirely in the direction of flow for the 5 μL/h experiments.

D^e ($\mu m^2/s$)	*Paenibacillus*	*Geobacter*	*Acidovorax*
1 μL/h	107 ± 46	308 ± 97	204 ± 56
5 μL/h	217 ± 43	895 ± 148	466 ± 74

3.1.3 Velocity Autocorrelation to Examine Emergence of Advection-Dominated Transport

We use the velocity autocorrelation function (C_v) to further provide information on advection-dominated transport [64]. Generally, in porous media, bacteria show decorrelation in velocities over time due to a tendency for sampling different portions of the flow field and trapping events (i.e., pore confinement, occurrence of collisions and attachment to obstacles) [8, 63]. Previous research has shown that decorrelation

of bacterial trajectories is more rapid at high flow rates [49]. Our findings both confirm these trends and present new information on how motility type impacts decorrelation. We show that *Paenibacillus* and *Acidovorax* exhibit decorrelation faster than *Geobacter* at 1 µL/h (Fig. 4a), but that at 5 µL/h, all decorrelation times are essentially the same. This suggests that at low flow rates swimmers experience larger variations in velocity over time by sampling multiple streamlines and trapping events that decorrelate subsequent velocities. However, as flow rate increases, motility type no longer has significant impact on decorrelation events. These observations further support the presence of flagella-based swimming for *Acidovorax* at 1 µL/h. Convergence of C_v decorrelation times at high flow rate points to the emergence of advection-dominated transport. These trends generally agree with the observations of the MSD, D^e and turn angle distribution analysis, although C_v is slightly less sensitive to differences in motility than the other metrics.

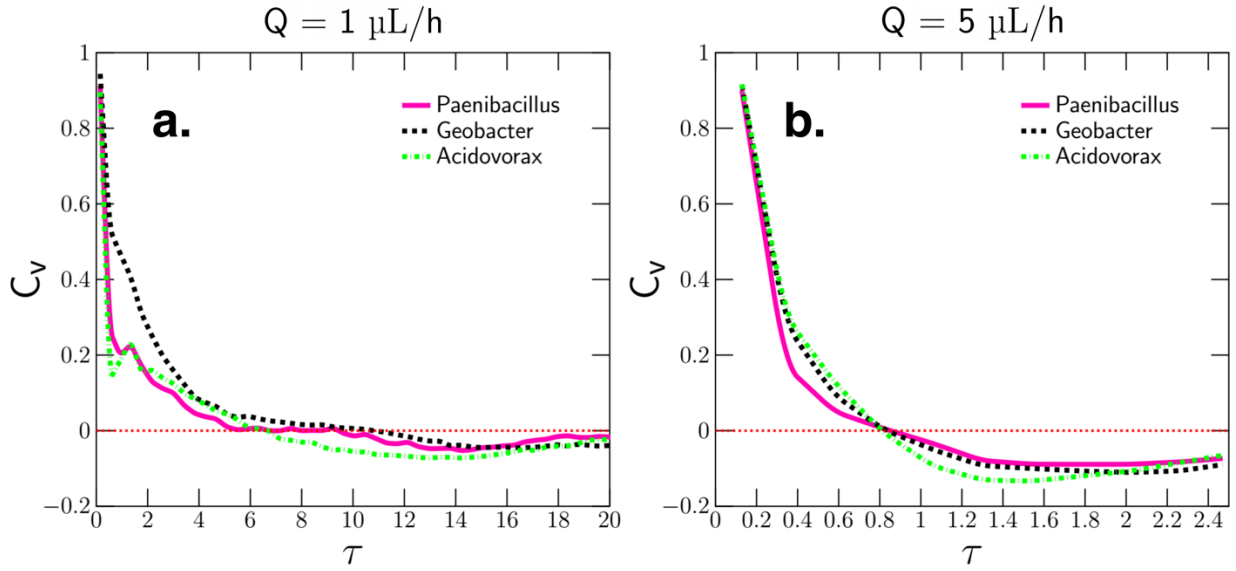

Figure 4. Velocity Autocorrelation functions (C_v) for the low porosity experiments at (a) 1 µL/h and (b) 5 µL/h. At 1 µL/h, the swimming species (*Paenibacillus* and *Acidovorax*) show faster decorrelation time (approximately 6.7 seconds) than the 10.8 second decorrelation time of the twitching species (*Geobacter*). At 5 µL/h the C_v for the plots of all species converges producing a decorrelation time of approximately 0.8 seconds, which is further evidence of advection-dominated transport.

3.2 Spatial Variations in Net Speeds

We digitized the experimental microfluidic geometries and simulated the steady-state viscous flow at high resolution using SimpleFoam [65, 66] to determine how bacteria may under or oversample different parts of a flow field (Fig. 5). By comparing the obtained simulated distribution of fluid speeds against the experimentally derived distribution of net bacterial speeds, we can develop an understanding of the zones within a pore network that bacteria may preferentially occupy. We recognize that a more accurate comparison would use flux weighting and particle tracking to compare the simulated fluid speed PDFs with

409 the net bacterial speed PDFs. However, given the large number of trajectories (tens of thousands for each
410 bacteria), and the periodic nature of our flow field, we posit that the trajectories of tracked bacteria
411 adequately sample the domain space and thus provide basis for comparison to simulated speeds.

412 We observe that regardless of flow rate, motility type, or porosity, motile bacteria in porous media tend to
413 undersample low-speed zones and oversample medium-speed zones (relative to the Eulerian fluid speed
414 PDF) (Fig. 6). This provides additional insight challenging the notion of shear trapping which suggests
415 bacteria in a shear flow will oversample low-speed zones [67, 68]. A plausible explanation for this observed
416 difference lies in recognizing that studies reporting shear trapping were often conducted in simpler
417 geometries (e.g., straight channels) [14] than in porous media geometries producing converging and
418 diverging streamlines, although it has been reported that shear may lead to creation of hotspot of
419 colonization instead of trapping close to walls of curved surfaces [18]. . An exact relationship between
420 hydrodynamics and the observed speed sampling cannot be

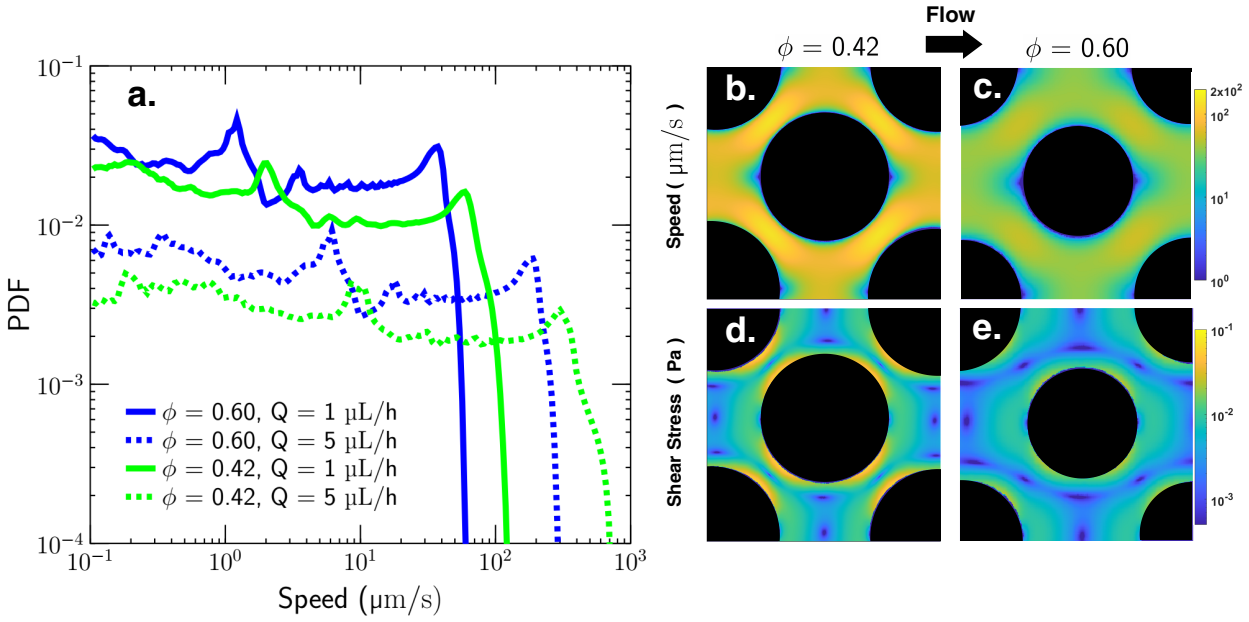

421

422 **Figure 5.** Results from the steady-state viscous flow simulations of our experimental microfluidic geometries. All low
423 porosity results in this figure are from the grain diameter = 80 μm, pore length = 20 μm geometry. **(a)** Probability
424 distribution functions (PDFs) of fluid speed from the simulated flow fields for each porosity and flow rate used in our
425 experiments. **(b)** Zoomed-in velocity magnitude field for the low porosity simulation at 1 μL/h. **(c)** Zoomed-in velocity
426 magnitude field for the high porosity simulation at 1 μL/h. **(d)** Zoomed-in shear stress magnitude field for the low
427 porosity simulation at 1 μL/h. **(e)** Zoomed-in shear stress magnitude field for the high porosity simulation at 1 μL/h.

428

429 deduced in our study because of lack of high-resolution tracking necessary to compute shear-induced lateral
430 transport towards the walls due to Jeffrey orbits [69-71] and potential backward swimming in the leeward
431 side of the grains, which has been reported has another form of shear trapping in more complex geometries
432 [18].

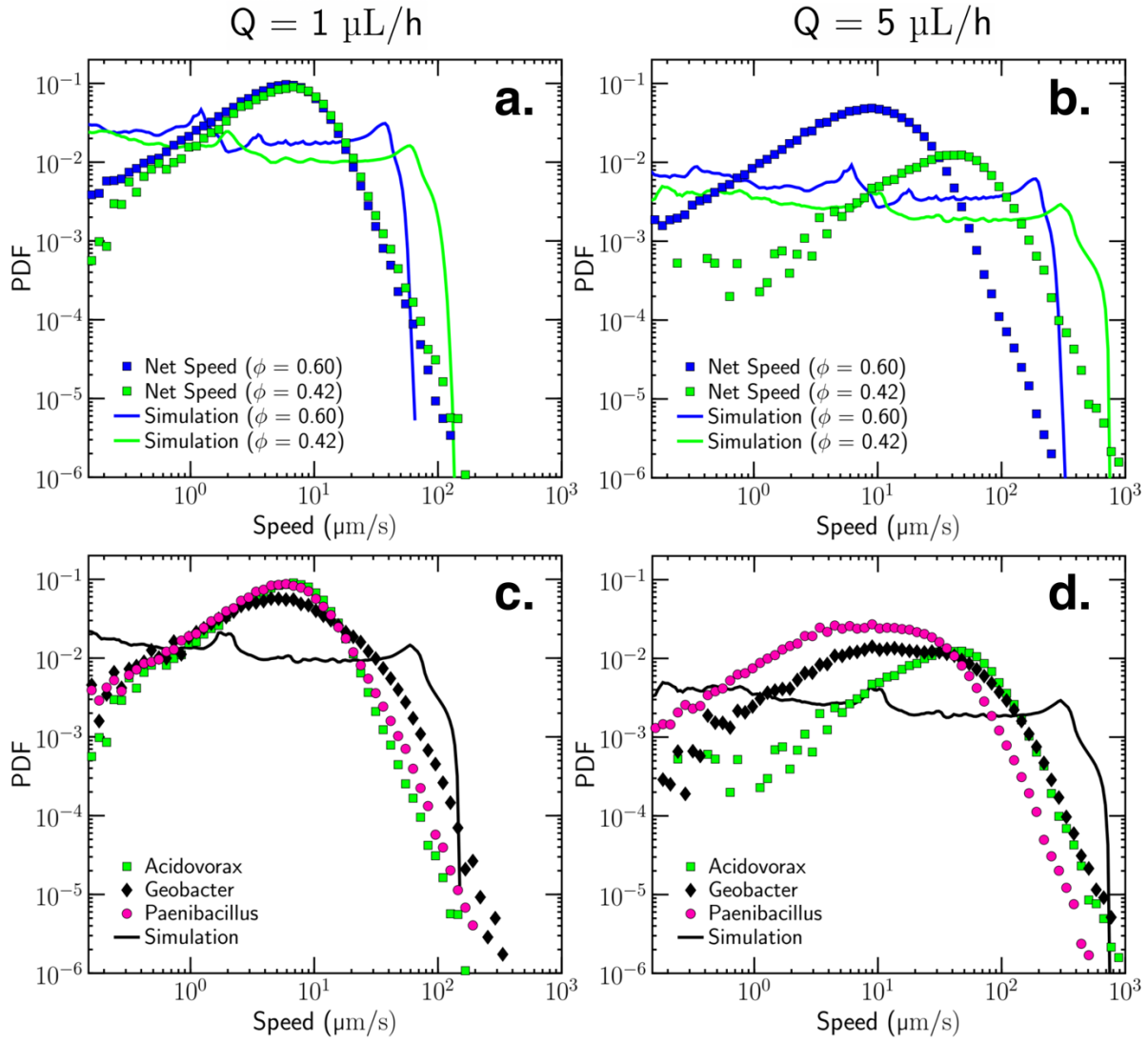

Figure 6. PDFs of speeds plotted to show the net speeds of the bacteria overlayed by the simulated speeds for the respective flow rate and porosity. The net speeds are represented by scatter points, whereas the simulated speeds are represented by solid lines. All low porosity results in this figure are from the grain diameter = 80 μm, pore length = 20 μm geometry. All simulated PDFs represent the distribution of Eulerian flow speeds for that geometry. **(a)** Net and simulated speed distributions for *Acidovorax* for $\phi = 0.60$ and $\phi = 0.42$ at a flow rate of 1 μL/h. **(b)** Net and simulated speed distributions for *Acidovorax* for $\phi = 0.60$ and $\phi = 0.42$ and flow rate of 5 μL/h. **(c)** Net and simulated speeds for all species for $\phi = 0.42$ at a flow rate of 1 μL/h. **(d)** Net and simulated speeds for all species for $\phi = 0.42$ at a flow rate of 5 μL/h. . These figures show the tendency for motile bacteria to oversample medium-speed zones within a porous media.

In no-flow conditions (Supplementary Fig 1), after subtracting drift speeds, *Geobacter* has a mean speed of 2.3 μm/s, *Acidovorax* has a mean speed of 5.9 μm/s, and *Paenibacillus* has a mean speed of 7.2 μm/s. The 95th percentile speed for the three species are 4.5 μm/s, 17.9 μm/s, and 20.6 μm/s for *Geobacter*, *Acidovorax*, and *Paenibacillus* respectively. At the low flow rate of 1 μL/h (16.5 μm/s average flow speed

at low porosity), the swimming speeds of *Acidovorax* and *Paenibacillus* can thus exceed the fluid flow speeds (although just barely in the case of *Acidovorax*), but at 5 μL/h, none of the bacteria in our study can consistently exceed the fluid flow speed. Thus, advection-dominated transport in its simplest form is a result of flow speeds exceeding motility speeds. However, shear adds another layer of complexity when considering the ability for bacteria to bundle/unbundle their flagella. Recent work has shown that at a shear magnitude of about 0.26 Pa, E. Coli lose control over this mechanism and can't effectively swim [72]. The 1 μL/h simulations in our study do not produce shear exceeding this value (Figs. 5d and 5e), but at 5 μL/h, the value of shear close to the grain is larger than this threshold value. Although an investigation of threshold shear magnitudes for bundling abilities in *Paenibacillus* and *Acidovorax* was beyond the scope of this paper, the inability to control motility [73] through bundling/unbundling of flagella remains a likely explanation for the differences observed in the transport of *Paenibacillus* and *Acidovorax*. It should be noted that in our quasi-2D porous media, under uniform and laminar flow, there are no chemotactic or thermal gradients influencing the transport. Thus, the magnitude and distribution of shear within a porous media, which attains its maximum value at grain surfaces and is minimum along centerlines of a pore channel, is likely the primary physical mechanism that controls bacterial transport.

3.3 Combined Effect of Turn Angle and Net Speed on Spreading

We further analyze the combined influence of net speed and turn angle on the advective spreading of motile bacteria using a matrix of bivariate (speed-angle) joint probability density contours (Fig. 7). The probability density matrix allows us to observe general relationships between the differential advection driven spreading plotted in Fig. 3a, and the turn angles and net speeds of the bacteria. As net speed increases, bacteria have a narrower range of turn angles and, therefore, greater spreading in the longitudinal direction stems from strongly advective particle motion. In the top and middle rows of Fig. 7, larger turn angles and less spreading are seen from left to right. In the bottom row, there is no significant change in large-angle turns or advective spreading. Thus, somewhere between the middle and bottom rows, or around a median speed of 50-100 μm/s, the impacts of advection-dominated transport increase to the extent that changes in fluid speed causes insignificant difference in advective spreading or turn angle for bacteria of the same motility type. This suppression in active dispersion in the case of strong fluid flow corroborates recent studies of transport of actively moving particles in porous media [74]. In addition to providing deeper insight into the transition to the advection-dominated regime, the joint probability density matrix also shows that bacteria are more likely to make large turns at low speeds than at high speeds. Conversely, small-angle turns are more likely to occur at high speeds than large-angle turns. When bacteria are moving with faster streamlines, their turn angles are smaller as they are more likely to go with the flow. When moving with slower streamlines, bacteria are more likely and more able to make large turns and cross transversely to other streamlines. This provides further evidence that pore space exploration and movement across streamlines require low fluid speeds and results in large turn angles.

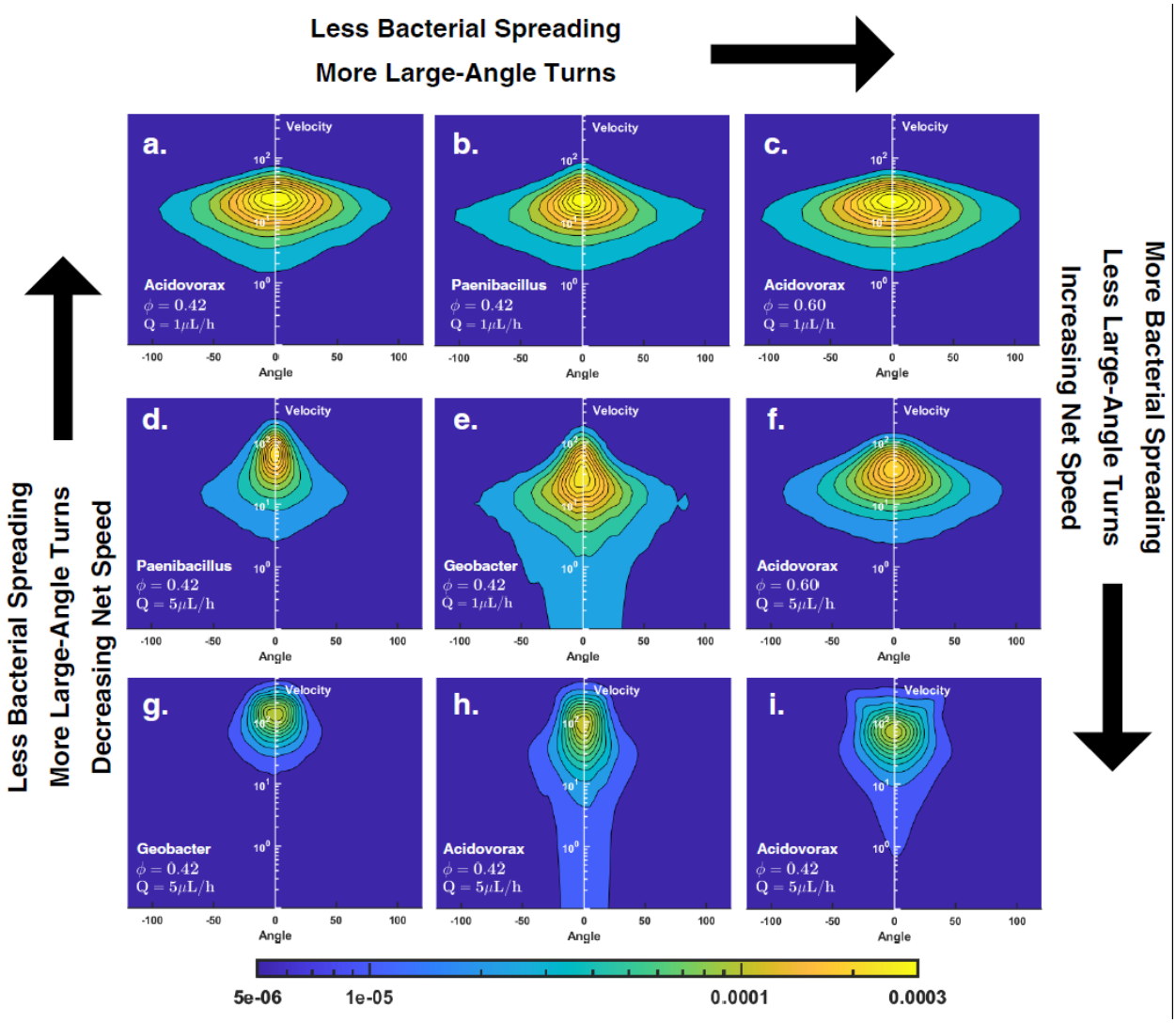

Figure 7. Velocity-angle joint probability density matrix. **(a)** *Acidovorax*, $\phi = 0.42$, 1 μL/h (grain diameter = 80 μm, pore length = 20 μm) **(b)** *Paenibacillus*, $\phi = 0.42$, 1 μL/h **(c)** *Acidovorax*, $\phi = 0.60$, 1 μL/h **(d)** *Paenibacillus*, $\phi = 0.42$, 5 μL/h **(e)** *Geobacter*, $\phi = 0.42$, 1 μL/h **(f)** *Acidovorax*, $\phi = 0.60$, 5 μL/h **(g)** *Geobacter*, $\phi = 0.42$, 5 μL/h **(h)** *Acidovorax*, $\phi = 0.42$, 5 μL/h (grain diameter = 80 μm, pore length = 20 μm) **(i)** *Acidovorax*, $\phi = 0.42$, 5 μL/h (grain diameter = 40 μm, pore length = 10 μm). Each figure in the density matrix shows probability density contours for net speed and turn angle for a particular set of conditions. As we move across the matrix from bottom to top, we see decreased net speeds, increased large-angle turns, and less spreading. As we move from left to right across the matrix, we see a slight increase in large-angle turns and decrease in spreading, but not as much as going from bottom to top. There is no significant change in net speed moving from left to right. This figure implies that fast net speeds are required for bacteria to be in the advection-dominated regime, which results in more small-angle turns. Furthermore, past a threshold speed of about 50-100 μm/s, motile bacteria are unlikely to have large-angle turns.

4. Discussion

This study focuses on investigating the impact of flow rates and porosity on the transport of different species of motile bacteria in porous media. We show that *Geobacter*, with their purely twitching-based motility, understandably need surfaces to propel themselves forward and are unable to swim in suspended media, and as a result are not fast enough in a porous media domain to show any impacts of motility on their transport at low or high flow rates. *Paenibacillus*, with their peritrichous flagella, exhibit strong swimming motility. Although they exhibit weak motion across streamlines and exploration of pore space at high flow rates, their turn angle distributions reflect a higher degree of activity. In the middle of the twitchers and swimmers are *Acidovorax*. Their transport metric are closer to swimmers at no-flow and at a flow rate of 1 μL/h, but at 5 μL/h, their transport metrics tend to appear closer to twitchers. Although a deep investigation of the motility type of *Acidovorax* is beyond the scope of this work, we show that differences in flagellar architecture offer a reasonable explanation for their behavior. Our results and previous imaging of *Acidovorax* suggest that they have a single polar flagellum as opposed to the peritrichous flagella of *Paenibacillus*. At high flow rates, it appears that peritrichous flagella are more able to facilitate tumbling behavior, and thus, movement across streamlines.

In the advection-dominated transport regime, lack of pore space exploration and streamline changing results in less transverse movement and thus leads to an overall increase in transported distance and spread in the direction of flow. We show that advection-dominated transport is revealed through convergence of turn angle distributions, MSDs, species independent velocity decorrelation times , and a clustering of turn angles around 0°. This study also provides contrasting results to the notion of shear trapping wherein motile bacteria are expected to oversample low-velocity regions in a shear flow. In the case of our complex porous geometry, we observe bacteria oversampling medium-speed regions. When the geometry of pore channels allows for convergence and divergence of streamlines in 2D space, producing hydrodynamic patterns typically found in realistic porous media, wide-ranging values of shear forces emerge, leading to an interesting interplay between shear, motility, and the overall bacterial transport. Oversampling of medium-speed zones could be because of high levels of shear (closer to the walls) preventing bacteria from bundling their flagella [72]. In this unbundled state, the bacteria act as deformable objects resulting in a stokes lift force as they approach surfaces. In addition, size exclusion and hydrodynamic chromatography have shown that the transport of microbes is dependent on size and shape [75, 76]. Size exclusion occurs because bacteria are too large to only occupy the slow speed zones around the grain [77]. Unless they are attached, bacteria will move more quickly around the grain than a solute will because part of their body is in higher speed zones. Finally, electrostatic repulsion, or the likely presence of energy barriers close to the grains, may prevent bacteria from getting too close to surfaces [18, 55, 78-81]. The wide variety of plausible explanations for absence of shear trapping in our study, or shear trapping being manifested at through bacterial reorientation in the leeward side of the grains, illustrate the complexities of analyzing bacterial transport in porous media. The oversampling of medium speeds can thus be a result of several different hydrodynamic or biophysical properties, and we identify shear as a likely physical phenomenon underpinning our observed transport patterns.

Our work complements previous studies that have shown advection to dominate the transport of bacteria at high flow rates [17, 25], effectively erasing the differences in motile behavior between different species of bacteria [14, 18, 67, 78, 82]. Our work also builds upon the body of evidence showing that there are significant transport differences between swimmers and twitchers [83, 84], and that bacteria with straighter paths (non-motile) spread more (in the direction of flow) than bacteria with exploratory paths (motile) at low flow speeds [17, 25]. We expect the results presented here to help future researchers in developing more robust experiments and models for not only bioremediation, but other applications where species-aware transport dynamics at small-scale can support and inform development of improved upscaled models. As evidenced by plots of various transport metrics which tend to move towards convergence at high flow rates, it can be argued at sufficiently high flow rates in porous media, different bacterial species will all exhibit uniform transport characteristics not too dissimilar than those expected from passive tracers. The usefulness of the presented research is in recognizing that such high flow rates are rarely encountered in porous media applications, and the progression of bacterial species towards a uniform transport behavior depends on the flow rates, porosities, and the motility types.

While we have tried to provide a robust analysis of bacterial transport in idealized porous media under different flow rates, we also recognize that our study contains many limitations. The bacteria were difficult to image and required large exposure times, which resulted in low frame rates and significant light scattering around the grains, thus impacting the accuracy of particle tracking. Furthermore, the low frame rate prevented us from analyzing bacteria through traditional run and tumble statistics. We also recognize that a more expansive set of experiments would have included a wider variety of flow rates (especially lower flow rates so that motility driven diffusion is more dominant than flow driven advection), which would allow for more confidence in any trends observed. Also, although we have mainly attributed the differences in transport of our three species to their differences in motility, there are other phenomena, such as the impact of hydrodynamics on different cell lengths (i.e., size exclusion), and DLVO and steric interactions [7], which could offer supporting explanations. A more rigorous study on the impacts of motility type would use mutant bacteria species that only differ in their motility types, which would allow for a more isolated observation of how motility affects overall transport. Finally, we recognize that a more complete study of the impacts of flow rate on the transport of different bacteria would examine the impact of shear on the ability for monotrichous and peritrichous flagella to bundle/unbundle. These limitations show that there is still significant work to be done to develop a mature theory of bacterial transport in porous media flows.

Data Availability

Besides the raw video and trajectory data, we have provided most of the other data and scripts required to replicate our findings in the supplementary materials. Raw video and trajectory data are available from the corresponding author upon reasonable request. The genome for *Acidovorax* JHL-9 can be found at: https://genome.jgi.doe.gov/portal/AcispJHL9_FD/AcispJHL9_FD.info.html.

Acknowledgments

This research is based upon work supported by the U. S. Department of Energy (DOE) under award number DE-SC0019437. The experiments were performed on a project award

(https://doi.org/10.46936/ltds.proj.2020.51218/60006749) from the Environmental Molecular Sciences Laboratory (EMSL), a DOE Office of Science User Facility sponsored by the Biological and Environmental Research program, and were partially supported by the Laboratory Directed Research and Development (LDRD) Program at Pacific Northwest National Laboratory. A portion of these data were produced by the US Department of Energy Joint Genome Institute (https://ror.org/04xm1d337; operated under Contract No. DE-AC02-05CH11231) in collaboration with the user community. The authors would specifically like to acknowledge the micromodel fabrication help received from Dr. Hardeep Mehta at EMSL and microscopy assistance from EMSL's Tom Wietsma. PNNL is a multi-program national laboratory operated for the U.S. Department of Energy (DOE) by Battelle Memorial Institute under Contract No. DE-AC05-76RL0-1830.

References

[1] Persat, A. Nadell, C.D., Kim, M.K., Ingremeau, F., Siryaporn, A., Drescher, K., Wingreen, N.S., Bassler, B.L., Gitai, Z., & Stone, H.A. The mechanical world of bacteria, *Cell* **161**, 988-997 (2015).

[2] Yang, P. & Van Elsas, J. D. Mechanisms and ecological implications of the movement of bacteria in soil. *Applied Soil Ecology* **129**, 112–120 (2018).

[3] Jalili-Firoozinezhad, S., Gazzaniga, F.S., Calamari, E.L., Camacho, D.M., Fadel, C.W., Bein, A., Swenor, B., Nestor, B., Cronce, M.J., Tovaglieri, A. & Levy, O. A complex human gut microbiome cultured in an anaerobic intestine-on-a-chip. *Nat Biomed Eng* **3**, 520–531 (2019).

[4] Mitchell, J. G. & Kogure, K. Bacterial motility: links to the environment and a driving force for microbial physics: Bacterial motility. *FEMS Microbiology Ecology* **55**, 3–16 (2006).

[5] Jakuszeit, T. & Croze, O.A. Role of tumbling in bacterial scattering at convex obstacles. *Physical Review E*, ***109*(4)**, 044405 (2024).

[6] Ugolini, G.S., Wang, M., Secchi, E., Pioli, R., Ackermann, M. & Stocker, R. Microfluidic approaches in microbial ecology. *Lab on a Chip* (2024).

[7] Tokárová, V., Sudalaiyadum Perumal, A., Nayak, M., Shum, H., Kašpar, O., Rajendran, K., Mohammadi, M., Tremblay, C., Gaffney, E.A., Martel, S. & Nicolau Jr, D.V. Patterns of bacterial motility in microfluidics-confining environments. *Proc. Natl. Acad. Sci. U.S.A.* **118**, e2013925118 (2021).

[8] Perez, L. J., Bhattacharjee, T., Datta, S. S., Parashar, R. & Sund, N. L. Impact of confined geometries on hopping and trapping of motile bacteria in porous media. *Phys. Rev. E* **103**, 012611 (2021).

[9] Bhattacharjee, T. & Datta, S.S. Confinement and activity regulate bacterial motion in porous media. *Soft Matter*, *15*(48), pp.9920-9930 (2019).

[10] Scheidweiler, D., Miele, F., Peter, H., Battin, T. J. & De Anna, P. Trait-specific dispersal of bacteria in heterogeneous porous environments: from pore to porous medium scale. *J. R. Soc. Interface.* **17**, 20200046 (2020).

[11] Makarchuk, S., Braz, V. C., Araújo, N. A. M., Ciric, L. & Volpe, G. Enhanced propagation of motile bacteria on surfaces due to forward scattering. *Nat Commun* **10**, 4110 (2019).

[12] Perez, L. J., Parashar, R., Plymale, A. & Scheibe, T. D. Contributions of biofilm-induced flow heterogeneities to solute retention and anomalous transport features in porous media. *Water Research* **209**, 117896 (2022).

[13] Ariel, G., Rabani, A., Benisty, S., Partridge, J.D., Harshey, R.M. & Be'Er, A. Swarming bacteria migrate by Lévy Walk. *Nat Commun* **6**, 8396 (2015).

[14] Rusconi, R., Guasto, J. S. & Stocker, R. Bacterial transport suppressed by fluid shear. *Nature Phys* **10**, 212–217 (2014).

[15] Barry, M. T., Rusconi, R., Guasto, J. S. & Stocker, R. Shear-induced orientational dynamics and spatial heterogeneity in suspensions of motile phytoplankton. *J. R. Soc. Interface.* **12**, 20150791 (2015).

[16] Yawata, Y., Nguyen, J., Stocker, R. & Rusconi, R. Microfluidic Studies of Biofilm Formation in Dynamic Environments. *J Bacteriol* **198**, 2589–2595 (2016).

[17] Creppy, A., Clément, E., Douarche, C., D'Angelo, M. V. & Auradou, H. Effect of motility on the transport of bacteria populations through a porous medium. *Phys. Rev. Fluids* **4**, 013102 (2019).

[18] Secchi, E., Vitale, A., Miño, G.L., Kantsler, V., Eberl, L., Rusconi, R. & Stocker, R. The effect of flow on swimming bacteria controls the initial colonization of curved surfaces. *Nat Commun* **11**, 2851 (2020).

[19] Rusconi, R., Lecuyer, S., Guglielmini, L. & Stone, H. A. Laminar flow around corners triggers the formation of biofilm streamers. *J. R. Soc. Interface.* **7**, 1293–1299 (2010).

[20] Rusconi, R., Lecuyer, S., Autrusson, N., Guglielmini, L. & Stone, H. A. Secondary Flow as a Mechanism for the Formation of Biofilm Streamers. *Biophysical Journal* **100**, 1392–1399 (2011).

[21] Pieper, D. H. & Reineke, W. Engineering bacteria for bioremediation. *Current Opinion in Biotechnology* **11**, 262–270 (2000).

[22] Ginn, T.R., Wood, B.D., Nelson, K.E., Scheibe, T.D., Murphy, E.M. & Clement, T.P. Processes in microbial transport in the natural subsurface. *Advances in Water Resources* **25**, 1017–1042 (2002).

[23] Scheidweiler, D., Bordoloi, A.D., Jiao, W., Sentchilo, V., Bollani, M., Chhun, A., Engel, P. & de Anna, P. Spatial structure, chemotaxis and quorum sensing shape bacterial biomass accumulation in complex porous media. *Nature Communications*, ***15*****(1),** 191 (2024).

[24] Song, J., Zhang, Y., Zhang, C., Du, X., Guo, Z., Kuang, Y., Wang, Y., Wu, P., Zou, K., Zou, L. & Lv, J. A microfluidic device for studying chemotaxis mechanism of bacterial cancer targeting. *Sci Rep* **8**, 6394 (2018).

[25] Dentz, M., Creppy, A., Douarche, C., Clément, E. & Auradou, H. Dispersion of motile bacteria in a porous medium. *J. Fluid Mech.* **946**, A33 (2022).

[26] Lee, J.H., Fredrickson, J.K., Plymale, A.E., Dohnalkova, A.C., Resch, C.T., McKinley, J.P. & Shi, L. An autotrophic H_2 -oxidizing, nitrate-respiring, Tc(VII)-reducing *Acidovorax* sp. isolated from a subsurface oxic-anoxic transition zone: H_2 -oxidizing, Tc-reducing *Acidovorax* spp. *Environmental Microbiology Reports* **7**, 395–403 (2015).

[27] Caccavo Jr, F., Lonergan, D.J., Lovley, D.R., Davis, M., Stolz, J.F. & McInerney, M.J. Geobacter sulfurreducens sp. nov., a hydrogen- and acetate-oxidizing dissimilatory metal-reducing microorganism. *Appl Environ Microbiol* **60**, 3752–3759 (1994).

[28] Ahmed, B., Cao, B., McLean, J.S., Ica, T., Dohnalkova, A., Istanbullu, O., Paksoy, A., Fredrickson, J.K. & Beyenal, H. Fe(III) Reduction and U(VI) Immobilization by Paenibacillus sp. Strain 300A, Isolated from Hanford 300A Subsurface Sediments. *Appl Environ Microbiol* **78**, 8001–8009 (2012).

[29] Krawczyk-Bärsch, E., Gerber, U., Müller, K., Moll, H., Rossberg, A., Steudtner, R. & Merroun, M.L. Multidisciplinary characterization of U(VI) sequestration by Acidovorax facilis for bioremediation purposes. *Journal of Hazardous Materials* **347**, 233–241 (2018).

[30] Methe, B.A., Nelson, K.E., Eisen, J.A., Paulsen, I.T., Nelson, W., Heidelberg, J.F., Wu, D., Wu, M., Ward, N., Beanan, M.J. & Dodson, R.J. Genome of *Geobacter sulfurreducens:* Metal Reduction in Subsurface Environments. *Science* **302**, 1967–1969 (2003).

[31] Govarthanan, M., Mythili, R., Selvankumar, T., Kamala-Kannan, S., Rajasekar, A. & Chang, Y.C. Bioremediation of heavy metals using an endophytic bacterium Paenibacillus sp. RM isolated from the roots of Tridax procumbens. *3 Biotech* **6**, 242 (2016).

[32] Jin, F., Conrad, J.C., Gibiansky, M.L. & Wong, G.C. Bacteria use type-IV pili to slingshot on surfaces. *Proceedings of the National Academy of Sciences*, ***108*****(31),** 12617-12622 (2011).

[33] Speers, A.M., Schindler, B.D., Hwang, J., Genc, A. & Reguera, G. Genetic identification of a PilT motor in Geobacter sulfurreducens reveals a role for pilus retraction in extracellular electron transfer. *Frontiers in microbiology*, **7**, 1578 (2016).

[34] Grady, E.N., MacDonald, J., Liu, L., Richman, A. & Yuan, Z.C. Current knowledge and perspectives of Paenibacillus: a review. *Microbial cell factories*, **15**, 1-18 (2016).

[35] Jayathilake, P.G., Li, B., Zuliani, P., Curtis, T. & Chen, J. Modelling bacterial twitching in fluid flows: a CFD-DEM approach. *Scientific reports*, **9(1),** 14540 (2019).

[36] Nakamura, S. Spirochete flagella and motility. *Biomolecules*, **10(4),** 550 (2020).

[37] Bahar, O., De La Fuente, L. & Burdman, S. Assessing adhesion, biofilm formation and motility of Acidovorax citrulli using microfluidic flow chambers. *FEMS Microbiology letters*, **312(1),** 33-39 (2010).

[38] Wang, S., Jaffe, P.R., Li, G., Wang, S.W. & Rabitz, H.A. Simulating bioremediation of uranium-contaminated aquifers; uncertainty assessment of model parameters. *Journal of Contaminant Hydrology*, ***64*****(3-4),** 283-307 (2003).

[39] Yabusaki, S.B., Fang, Y., Williams, K.H., Murray, C.J., Ward, A.L., Dayvault, R.D., Waichler, S.R., Newcomer, D.R., Spane, F.A. & Long, P.E. Variably saturated flow and multicomponent biogeochemical reactive transport modeling of a uranium bioremediation field experiment. *Journal of contaminant hydrology*, ***126*****(3-4),** 271-290 (2011).

[40] Liu, Y., Du, M., Shu, S., Wei, J., Zhu, K. & Wang, G. Bacterial surface properties and transport behavior actively respond to an extracellular polymeric substance gradient in saturated porous media. *Science of The Total Environment*, 173889 (2024).

690 [41] Yang, X., Parashar, R., Sund, N.L., Plymale, A.E., Scheibe, T.D., Hu, D. & Kelly, R.T. On Modeling
691 Ensemble Transport of Metal Reducing Motile Bacteria. *Sci Rep* **9**, 14638 (2019).

692 [42] Tinevez, J.Y., Perry, N., Schindelin, J., Hoopes, G.M., Reynolds, G.D., Laplantine, E., Bednarek, S.Y.,
693 Shorte, S.L. & Eliceiri, K.W. TrackMate: An open and extensible platform for single-particle tracking.
694 *Methods* **115**, 80–90 (2017).

695 [43] Lovley, D.R., & Phillips, E.J.P. Novel mode of microbial energy metabolism: organic carbon oxidation
696 coupled to dissimilatory reduction of iron or manganese. *Appl. Environ. Microbiol.* **54**, 1472-1480 (1988).

697 [44] Plymale, A.E., Bailey, V.L., Fredrickson, J.K., Heald, S.M., Buck, E.C., Shi, L., Wang, Z., Resch,
698 C.T., Moore, D.A. & Bolton Jr, H. Biotic and Abiotic Reduction and Solubilization of Pu(IV)O2•xH2O(am)
699 as Affected by Anthraquinone-2,6-disulfonate (AQDS) and Ethylenediaminetetraacetate (EDTA). *Environ.*
700 *Sci. Technol*. **46**, 2132–2140 (2012).

701 [45] Lin, W. C., M. V. Coppi, & Dr. R. Lovely. Geobacter sulfurreducens Can Grow with Oxygen as a
702 Terminal Electron Acceptor. *Appl. Environ. Microbiol.* **70 (4)**, 2525-2528 (2004).

703 [46] Thornton, M.M., Chung-Esaki, H.M., Irvin, C.B., Bortz, D.M., Solomon, M.J. & Younger, J.G.
704 Multicellularity and antibiotic resistance in Klebsiella pneumoniae grown under bloodstream-mimicking
705 fluid dynamic conditions. *The Journal of infectious diseases*, **206(4),** 588-595 (2012).

706 [47] Tuval, I., Cisneros, L., Dombrowski, C., Wolgemuth, C.W., Kessler, J.O. & Goldstein, R.E. Bacterial
707 swimming and oxygen transport near contact lines. *Proceedings of the National Academy of Sciences*,
708 **102(7),** 2277-2282 (2005).

709 [48] Rossy, T., Nadell, C.D. & Persat, A. Cellular advective-diffusion drives the emergence of bacterial
710 surface colonization patterns and heterogeneity. *Nature communications*, **10(1),** 2471 (2019).

711 [49] Dehkharghani, A., Waisbord, N., Dunkel, J. & Guasto, J.S. Bacterial scattering in microfluidic crystal
712 flows reveals giant active Taylor–Aris dispersion. *Proceedings of the National Academy of Sciences*,
713 **116(23),** 11119-11124 (2019).

714 [50] Einstein, A. On the Movement of Small Particles Suspended in Stationary Liquids Required by the
715 Molecular-Kinetic Theory of Heat. *Annalen Der Physik*, 549–560 (1905).

716 [51] Duffy, K. J. & Ford, R. M. Turn angle and run time distributions characterize swimming behavior for
717 Pseudomonas putida. *J Bacteriol* **179**, 1428–1430 (1997).

718 [52] Berg, H.C. & Brown, D.A. Chemotaxis in Escherichia coli analysed by three-dimensional tracking.
719 *Nature*, **239(5374),** 500-504 (1972).

720 [53] Becker, M. W., Metge, D. W., Collins, S. A., Shapiro, A. M. & Harvey, R. W. Bacterial Transport
721 Experiments in Fractured Crystalline Bedrock. *Ground Water* **41**, 682–689 (2003).

722 [54] Liu, J., Ford, R. M. & Smith, J. A. Idling Time of Motile Bacteria Contributes to Retardation and
723 Dispersion in Sand Porous Medium. *Environ. Sci. Technol.* **45**, 3945–3951 (2011).

724 [55] Conrad, J. C. & Poling-Skutvik, R. Confined Flow: Consequences and Implications for Bacteria and
725 Biofilms. *Annu. Rev. Chem. Biomol. Eng.* **9**, 175–200 (2018).

[56] Dehkharghani, A., Waisbord, N. & Guasto, J.S. Self-transport of swimming bacteria is impaired by porous microstructure. *Commun Phys* **6**, 18 (2023).

[57] Ford, R.M. & Harvey, R.W. Role of chemotaxis in the transport of bacteria through saturated porous media, *Advances in Water Resources* **30**(6-7): 1608-1617 (2008).

[58] Bente, K., Mohammadinejad, S., Charsooghi, M.A., Bachmann, F., Codutti, A., Lefèvre, C.T., Klumpp, S. & Faivre, D. High-speed motility originates from cooperatively pushing and pulling flagella bundles in bilophotrichous bacteria. *Elife*, **9**, e47551 (2020).

[59] Najafi, J., Shaebani, M.R., John, T., Altegoer, F., Bange, G. & Wagner, C. Flagellar number governs bacterial spreading and transport efficiency. *Sci Adv* **4**: eaar6425 (2018).

[60] Mitchell, J.G. The energetics and scaling of search strategies in bacteria. *The American Naturalist,* **160(6),** 727-740 (2002).

[61] Kaya, T. & Koser, H. Direct upstream motility in Escherichia coli. *Biophysical journal*, **102(7),** 1514-1523 (2012).

[62] Perez, L.J., Hidalgo, JJ., & Dentz, M. Upscaling of mixing-limited bimolecular chemical reactions in Poiseuille flow. *Water Resources Research* **55**, no. 1: 249-269 (2019).

[63] Puyguiraud, A., Perez, L.J., Hidalgo, JJ., & Dentz, M. Effective dispersion coefficients for the upscaling of pore-scale mixing and reaction. *Advances in Water Resources* **146**: 103782 (2020).

[64] Weber, S.C., Thompson, M.A., Moerner, W.E., Spakowitz, A.J., & Theriot, J.A. Analytical tools to distinguish the effects of localization error, confinement, and medium elasticity on the velocity autocorrelation function. *Biophysical journal*, **102**(11), 2443-2450 (2012).

[65] Weller, H. G., Tabor, G., Jasak, H. & Fureby, C. A tensorial approach to computational continuum mechanics using object-oriented techniques. *Comput. Phys.* **12**, 620 (1998).

[66] OpenFOAM Foundation. OpenFOAM: Open-source CFD software. Retrieved from https://openfoam.org/ (2023).

[67] Vennamneni, L., Nambiar, S., & Subramanian, G. "Shear-induced migration of microswimmers in pressure-driven channel flow." *Journal of Fluid Mechanics* 890: A15 (2020).

[68] Lee, M., Lohrmann, C., Szuttor, K., Auradou, H. & Holm, C. The influence of motility on bacterial accumulation in a microporous channel. *Soft Matter*, **17(4),** 893-902 (2021).

[69] Jeffery, G.B. The motion of ellipsoidal particles immersed in a viscous fluid. *Proceedings of the Royal Society of London.* Series A, Containing papers of a mathematical and physical character, **102(715),** 161-179 (1922).

[70] Pedley, T.J. & Kessler, J.O. Hydrodynamic phenomena in suspensions of swimming microorganisms. *Annual Review of Fluid Mechanics*, **24(1),** 313-358 (1992).

[71] Choudhary, A., Paul, S., Rühle, F. & Stark, H. How inertial lift affects the dynamics of a microswimmer in Poiseuille flow. *Communications Physics*, **5(1),** 14 (2022).

[72] Yang, J., Kikuchi, K. & Ishikawa, T. High shear flow prevents bundling of bacterial flagella and induces lateral migration away from a wall. Communications Physics, **6(1),** 354 (2023).

[73] Licata, N.A., Mohari, B., Fuqua, C. & Setayeshgar, S. Diffusion of bacterial cells in porous media. *Biophysical journal*, **110(1),** 247-257 (2016).

[74] Alonso-Matilla, R., Chakrabarti, B. a& nd Saintillan, D. Transport and dispersion of active particles in periodic porous media. *Physical Review Fluids*, **4(4),** 043101 (2019).

[75] Weiss, T.H., Mills, A.L., Hornberger, G.M. & Herman, J.S. Effect of bacterial cell shape on transport of bacteria in porous media. *Environmental science & technology*, **29(7),** 1737-1740 (1995).

[76] Fontes, D.E., Mills, A.L., Hornberger, G.M. & Herman, J. Physical and chemical factors influencing transport of microorganisms through porous media. *Applied and Environmental Microbiology,* **57(9),** 2473-2481 (1991).

[77] F. Grant Ferris; Natalie Szponar; & Brock A. Edwards. Groundwater Microbiology. *The Groundwater Project* (2021).

[78] Molaei, M. & Sheng, J. Succeed escape: Flow shear promotes tumbling of Escherichia colinear a solid surface. *Sci Rep* **6**, 35290 (2016).

[79] Johnson, W. P., Blue, K. A., Logan, B. E. & Arnold, R. G. Modeling Bacterial Detachment During Transport Through Porous Media as a Residence-Time-Dependent Process. *Water Resour. Res.* **31**, 2649–2658 (1995).

[80] Dong, H., Scheibe, T. D., Johnson, W. P., Monkman, C. M. & Fuller, M. E. Change of Collision Efficiency with Distance in Bacterial Transport Experiments. *Ground Water* **44**, 415–429 (2006).

[81] Hermansson, M. The DLVO theory in microbial adhesion. *Colloids and Surfaces B: Biointerfaces* **14**, 105–119 (1999).

[82] de Anna, P., Pahlavan, A.A., Yawata, Y., Stocker, R. & Juanes, R.. Chemotaxis under flow disorder shapes microbial dispersion in porous media. *Nat. Phys.* **17**, 68–73 (2021).

[83] Son, K., Brumley, D.R., & Stocker, R. Live from under the lens: exploring microbial motility with dynamic imaging and microfluidics. *Nature Reviews Microbiology*. **13**, 761–775 (2015).

[84] Lu, N., Bevard, T., Massoudieh, A., Zhang, C., Dohnalkova, A.C., Zilles, J.L. & Nguyen, T.H. Flagella-Mediated Differences in Deposition Dynamics for Azotobacter *vinelandii* in porous media. *Environ. Sci. Technol*. **47**, 5162–5170 (2013).

Supplementary Figures

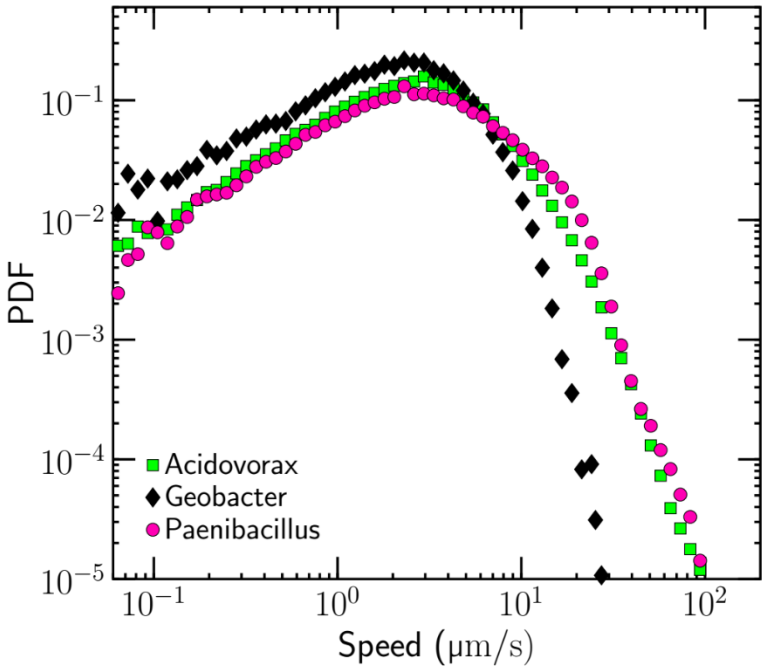

Supplementary Figure 1. Speed PDF for no-flow experiments in the high porosity geometry (grain diameter = 40 μm, pore length = 20 μm).

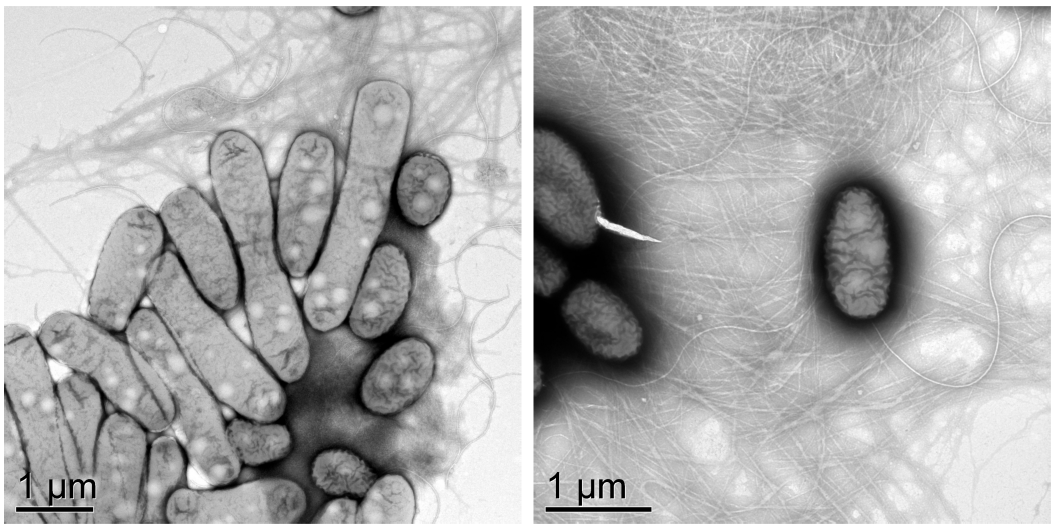

Supplementary Figure 2. Whole-mount transmission electron microscopy (TEM) images of *Acidovorax* JHL-9 (unpublished images from [26], courtesy of Alice Dohnalkova). The whole-mount images were prepared by adding JHL-9 liquid culture to a copper electron microscopy grid and examining by TEM at 200 kV using a JEOL 2010 high-resolution TEM.